Lawrence Berkeley Laboratory
UNIVERSITY OF CALIFORNIA

Physics, Computer Science & Mathematics Division

Presented at the International School of Radiation Damage and Protection, Ettore Majorana Center for Scientific Culture, Erice, Sicily, September 16-26, 1979; and to be published in the Proceedings,"Advances in Radiation Protection and Dosimetry in Medicine", V. Perez-Mendez and R. Thomas, eds. Plenum Pub.

ADVANCES IN DIAGNOSTIC INSTRUMENTATION

Victor Perez-Mendez

January 1980

Prepared for the U.S. Department of Energy under Contract W-7405-ENG-48

DISCLAIMER

ADVANCES IN DIAGNOSTIC INSTRUMENTATION

Victor Perez-Mendez

Lawrence Berkeley Laboratory
Berkeley, CA 94720

University of California, San Francisco
San Francisco, CA 94143

INTRODUCTION

The art of medical diagnosis is a continuously evolving process which often owes its progress to technical developments in other scientific fields.

The major advance in Radiology during the last ten years has been the development of Computerized Tomography. Although many of the principles of this technology have been known for considerably longer periods of time, the actual implementation became feasible only with the development of versatile high speed small computers with large memory storage capacities at modest prices. Other technological developments which made C. T. a reality were (a) advances in Applied Computational Mathematics such as the Fast Fourier Transform algorithms, as well as graphic display programs, and (b) developments in new photon detectors.

These advances in diagnostic x-ray imaging have had their influence in other branches of Radiology, such as Nuclear Medicine and Ultrasonography.

Nuclear medicine provides complementary information to x-ray diagnosis in that it provides information on the vascular and physiological processes that distribute a given radioisotope-labelled compound within the desired organ. The possibility of obtaining tomographical information on the concentration distribution of the radioisotope distribution was recognized even earlier than in the x-ray case. Its implementation is now taking place, although at a

slower rate than with the Transmission Computerized Tomography.

Ultrasonography is an imaging technique which is also undergoing rapid new developments. A major impetus to its expanded use is the fact that it does not involve ionizing radiation, and at the intensity levels which are under use, is not known to create any cell damage. The present techniques, which are almost duplicates of older Radar imaging concepts, provide a Tomographic image in the well known B-scan approach. However, Radar imaging with the aid of more elaborate electronics to provide faster and more accurate pattern recognition is now providing the technological basis for advances in Ultrasound Imaging.

Lastly, the well known x-ray tube itself has recently undergone improvements in design that permit higher quality transmission x-ray pictures. In order to detect smaller structures or more detail in a transmission image, it is necessary to magnify the image either in the x-ray projection or by enlarging the resultant film. Principles of electron beam focussing taken from electron accelerator technology have played a role in this development.

Table I lists the topics covered in this paper. Other diagnostic imaging concepts involving Nuclear Magnetic Resonance (NMR), Thermography (infrared and microwave), as well as Electrical Impedance C. T., are areas in which there is a lot of research activity at present.

Table I. Developments in Medical Imaging

1) Fine Focus X-ray Tubes
   a) Structure of Electron Gun
   b) Resolution Patterns

2) Computerized Tomography: X-ray Transmission
   a) Configurations of C. T. Machines: 2π Geometry
   b) Fast C. T, Machines: Limited Fan Angle Geometry
   c) Principles of Limited Angle Reconstructions

3) Emission Tomography: Radioisotope Imaging
   a) Single Photon Emission Tomography
   b) Positron Imaging: Planar and 2π Ring Cameras

4) Ultrasound Imaging
   a) Grey Scale B-scan Principles
   b) Phased Array Transducers: Electronic Steering and Focussing
   c) Real Time B-scans.

HIGH RESOLUTION RADIOLOGY

The technology of x-ray tube construction and performance is obviously one to which the manufacturers place close attention. In this section we discuss one recent approach to high resolution x-ray tubes which provide a focal spot at the anode of the tube smaller than 90 microns. The heat dissipation limits the maximum power that can be used and hence the maximum x-ray exposure.

Figure 1a shows a conventional medium power x-ray tube using a metal focussing cup around the cathode. Tubes of this type have focal spots ranging from 0.5-3 mm, depending on the power used. A method used to produce a smaller focal spot [1] involves building the tube with a series of focussing grids, as shown in Fig. 1b, that can focus the electron beam to spots smaller than 80 microns. Since x-ray pictures are projections of the transmission from the source (x-ray tube) through the object to the film, the overall resolution depends on the geometrical spacing of all three, with the limitation being the effective dimensions of the x-ray source. High resolution x-ray pictures are of use in studying bone structures as shown in Fig. 2a. Another application in which high resolution x-ray imaging has been used recently is in the diagnosis of breast tumors by showing the existence of small calcifications ranging in size from 0.3 mm to a few mm in size. Malignant tumors of the breast are often associated with the smaller calcifications [2], a sample of which is shown in Fig. 2b.

COMPUTERIZED TOMOGRAPHY

Tomography is the name given to the process by which a three-dimensional object can be displayed graphically as a series of slices. In medical diagnosis there are presently in use the tomographic procedures defined in Table II and illustrated in Fig. 3.

X-ray C. T. is achieved by detecting electronically the transmission of the x-ray beam through an object when viewed from a series of angles. One slice of the object is measured at a time: the x-ray source is moved around 2π angle around the object. Various computational algorithms involving Fourier Transforms are used in reconstructing the image on matrices with size up to 300 x 300 picture elements called Pixels. Fig. 4 shows configurations of various x-ray C. T. machines. The first successful C. T. machine, the EMI head scanner of 1973, accomplished the multidirectional viewing by using a parallel beam geometry with a single sodium iodide crystal detector, moved in a combination of translational and rotational motions.

This slow (~5 min./scan) machine was replaced next by a fan beam geometry in which a series of detectors recorded the attenuation

Table II. Medical Tomography

Tomography: Greek word meaning "to take a slice," in this case to take a 3-D object and display graphically as a series of slices.
Computerized Tomography (X-ray C. T.)L Display density distribution of body (organ) section.
Ultrasound B-scan: Display tissue boundaries of body (organ) sections.
Emission Tomography: Display concentration distribution of gamma-emitting radioisotope in organ section.

of the beam from the x-ray source through the object. The x-ray tube and the detector array moved jointly along the periphery of a mechanical gantry. This arrangement proved to be unsatisfactory in that any slight inhomogeneity in the gain of the detectors provided circular artifacts on the image. This difficulty was eliminated in the "fourth generation" scanner in which 200-300 idividual detectors are mounted on a circular gantry; the x-ray tube alone moves. The gain of each detector in the bank is adjusted electronically on each rotation. This scheme eliminated most circular artifacts.

In earlier machines, the detectors were xenon gas ionization chambers; in some of the newer C. T. machines there are now sodium iodide scintillation counters. Some newer machines will use bismuth germanate scintillation crystals, since their detection efficiency is higher than that of sodium iodide (due to the high Z of the bismuth). Also, bismuth germanate crystals do not have the low intensity, long-term fluoresence that sodium iodide has and therefore favors the main objective of newer C. T. machines, which is to provide higher resolution images during a shorter period of time. This is necessary in order to accomplish dynamic imaging of the heart in motion.

Fig. 5a shows a picture of the General Electric fast scanner in research use in the Radiology Department, University of California, San Francisco [3]. This machine, a fourth generation scanner, produces two 180° images during a single 2.4 sec, 360° revolution. Following a 1 sec pause the scanner reverses direction and scans back in 2.4 sec. This sequence is repeated until 12 images at approximately 1.5 sec intervals have been produced. Fig. 5b shows the kind of star artifact that can appear in a scan if a high density object such as a metal clip is present.

Comparable fast scanners have been made by other manufacturers

in various countries. The fastest scanner under development is one at the Mayo Clinic that will provide 60 images/sec, each of 0.01 sec duration [4]. In order to accomplish this, the machine uses 28 x-ray tubes which are pulsed sequentially. Another approach to fast C. T. machines is the use of a rotating focussed high voltage electron beam. Two such schemes are shown in Fig. 6; Fig. 6a [5] shows a proposed machine in which the electron beam is rotated over the full 360° and Fig. 6b shows a scheme in which the beam and detector cover only 180° [6].

The fact that it is possible to obtain good tomographic reconstructions using scanners that cover less than the full 2π angle in a plane is illustrated in Fig. 7. In the more general case, it is possible to reconstruct the density distribution within a volume from projections that cover less than 4π solid angle. For simplicity, we discuss the planar case for transmission tomography. The mathematical concepts apply also to Radioisotope-Emission Tomography, discussed in the next section, and to other fields of science such as electron microscopy and radioastronomy.

The feasibility of high quality tomographic reconstruction from limited-angle input data rests on the following theorems: (a) The "Projection Theorem" states that the integral of the absorption of radiation along a straight line through the object determines the Fourier components of the density along a line in Fourier space perpendicular to the projection direction [7]. This theorem holds also for the case of a radiation-emitting object where the concentration distribution of the emitter is to be obtained from the measurements. (b) The Fourier Transform of a finite object with a finite maximum density is an entire function in the Fourier domain, hence knowledge of the F. T. in any finite region of the Fourier space implies knowledge of the F. T. over all the remaining space.

One way to obtain the complete F. T. over all spatial frequency space from the directly measured cone, as shown in Fig. 7, is to perform the reconstruction by an iterative procedure that starts off with the measured values K_x, K_y in the allowed cone and K_x, K_y = 0 outside it. By a series of iterations that use the restriction that the object has a non-negative density within its bounded volume and is zero outside, it is possible to calculate the missing components with an accuracy that depends on the size of the angle θ and the statistical quality of the measured data [8]. Other reconstruction methods are described in a special issue of the IEEE Trans. Nuc. Sci. 26, no. 2 (April 1979).

EMISSION TOMOGRAPHY: RADIOISOTOPE IMAGING

Nuclear Medicine is the diagnostic imaging discipline that uses gamma-emitting isotopes to trace physiological abnormalities within

a given organ. Using scintillation cameras with various types of collimators to image a projection of the radioisotope concentration within the organ, it has supplied useful complementary information to the x-ray diagnosis.

Obviously, if the concentration of isotope can be determined in tomographic layers, greater contrast in detecting abnormalities would be achieved. A straight forward method of obtaining tomographic reconstructions with gamma-emitting isotopes is shown in Fig. 8a [9]. The organ in question is viewed from a 2π angular range by taking images at a series of angles with a scintillation camera equipped with a parallel-hole collimator. However, the procedure is time consuming, and the equipment is rather bulky.

A newer approach, for the specific purpose of obtaining tomographic images of the myocardium, was developed at the Denver Veterans Administration Hospital [10]. A seven-pinhole collimator was mounted on a large scintillation camera (LFOV: diameter of NaI crystal = 40 cms) in such a way that seven non-overlapping images of the heart were obtained, as shown in Fig. 8b. The conventional radioisotope for this purpose, ^{201}Thallium (E_γ = 60-80 keV), was used. The information of the separate images was stored on a computer. Since the independent images view the heart from a range of different angles, it is possible to obtain tomographical reconstructions as shown in Fig. 9. This method is limited to tomographical scans of small organs, since the seven separate images have to be recorded with adequate resolution on the detector and without overlapping each other.

Another approach to Radioisotope Emission Tomography is to use the 511 keV gamma-rays from the annihilation of positron-emitting isotopes at rest. This approach was suggested as early as 1953, but it is only during the last few years that it has been used clinically. This became possible primarily because of detector and computer development, and also because of the impetus given to tomographical imaging in general by the success of the C. T. machines in Radiology.

Positron annihilation tomography has the following advantages over single photon tomography:

a) The two 511 keV annihilation gamma-rays come off at 180° when the positrons annihilate at rest; the mean angle is 180° $\pm$ 0.5°, where the angular spread is due to annhilation by electrons in motion. When the two gammas are detected in coincidence, the position of the emitting atom is known to be on this line. This is shown schematically in Fig. 10a. This fact eliminates the need to use a collimator for defining the direction of the gamma rays, as indicated in Fig. 10b. Since the transmission of a collimator used

in single photon imaging is approximately 10^{-4} its absence allows the use of smaller doses for the positron imaging case.

b) The only reasonably long-lived "gamma-emitting" isotopes of C, O, N are positron emitters. Furthermore, parent-daughter generators of positron-emitting isotopes are available, such as ^{68}Ge (250d) $\rightarrow$ ^{68}Ga (1.1 hr) and ^{82}Sr (25d) $\rightarrow$ ^{82}Rb (1.2 m), which can fulfill most imaging requirements.

Positron cameras can be built in two configurations: (a) as two large-area detectors (Fig. 10b) which cover a limited fraction of 4π solid angle; and (b) ring cameras (Fig. 10c), as built by Donner Laboratory, University of California, Berkeley [11], Washington University [12], University of California, Los Angeles [13], McGill [14], and others. Cameras of the first category use two scintillation cameras [15] or two multicrystal cameras [16] or MWPC detectors with converters [17,18]. The ring cameras cover 2π solid angle in one plane and can measure one or more planes at a time.

In Fig. 11a we show some construction details of the Donner Laboratory 280 NaI crystal camera; Fig. 11b shows a representative heart scan taken with ^{82}Rb. The NaI crystals will be replaced by Bismuth Germanate crystals in order to increase the detection efficiency.

In Fig. 12 we show the principles of a multiwire proportional chamber camera. The MWPC is capable of recording the position of an ionizing event by the signals induced on the orthogonal cathode grids of wires on either side of the anode wire plane. When the ionizing event is a charged particle from an external source, position accuracy measured on the cathode grids is less than 0.5 mm.

In order to detect 511 keV gamma-rays with reasonable efficiency high Z element converters from which the interaction electrons can be extracted to form avalanches on the anode wires have to be placed within the chamber. Fig. 12a shows a cross-sectional layout of such a chamber as built at the Lawrence Berkeley Laboratory. The efficiency of a converter from which electrons can be extracted depends on maximizing the useful-surface area to volume. Fig. 12c shows converters that were used in this camera. They consist of a series of lead platings on plastic backing, corrugated to form holes of approximately 3.5 mm diameter. The insulated strips are necessary so that a suitable electric field can be placed across them to drift the interaction electrons out of the converter region and into the sensitive area of the MWPC between the cathode and anode planes. A more efficient converter can be made by using matrices of high lead content glass (80% PbO) tubes with holes approximately 1.4 mm in diameter. The glass surface is made resistive by hydrogen reduction at high temperatures. Then a voltage of 500 V/cm will produce a suitable electric field for drifting the electrons [19]. Other

schemes for converters are to etch small holes on stacks of thin lead foils with thin plastic insulated layers between them [20] or to make arrays of tungsten wires (Prague University, Massachusetts Institute of Technology).

In Fig. 13 we show schematically the configuration of a MWPC camera and a head scan of a tumor region imaged with a ^{68}Ga compound and reconstructed on a series of four planes.

ULTRASOUND IMAGING

In this section we discuss the present methods that are used in producing the essentially tomographic images of body structures as a B-scan, and recent developments [21].

B-scans are usually done by sending a succession of short ultrasonic pulses at a series of overlapping directions into the patient's body. One planar cross-section of the body is displayed on an oscilloscope screen at any one time. This is accomplished in diagnostic scanners by having the transducer mounted on a hinged arm that permits motion in a single plane, producing a scan such as that shown in Fig. 14a. The frequency of ultrasound in clinical imaging is 2.25-3.5 MHz, limited at the high side by the increasing attenuation of sound propagation at higher frequencies.

The technique is very similar to Radar ranging. A short pulse of sound is sent along a given direction. Any reflecting surface in its path will send back a signal at the appropriate angle for specular reflection. If the surface is perpendicular to the sound direction, the reflected signal will be detected at a delayed time, which is proportional to the distance on the send transducer, by the inverse piezoelectric effect.

The amplitude of the reflected signal, after time-gated amplifier gain correction for the attenuation in the medium, depends on the coefficient of reflection

$$\mathcal{E} = I_{Ref}/I_{Send} \qquad \mathcal{E} = (\rho_1 V_1 - \rho_2 V_2)^2/(\rho_1 V_1 + \rho_2 V_2)^2$$

where ρ_1, ρ_2, V_1, and V_2 are the densities and velocities of sound of the two media at the interface. The reflection coefficient drops off by a factor of approximately ten within 5° of the perpendicular direction.

Older diagnostic machines produced a bi-stable picture. In this case, a fixed intensity dot was produced on the oscilloscope screen whenever the reflected signal exceeded a preset level. Scans of this type tended to be rather "spotty" with sections of surfaces missing if their inclination was too far away from the specular

backward reflection angle. However, boundaries such as foetal heads, where distance measurements are taken to record growth, were very precisely delineated. Partial filling in of scattering from inclined surfaces can be achieved by using a logarithmic gain amplifier to display dots on the oscilloscope screen, whose intensity is correlated with the reflected amplitude. These "Grey scale" images fill in more of the boundary details and density anomalies within the organs. If the Grey scale gain controls are misused, the resulting scans can either be too full of reflections or omit low-contrast details.

Recent developments in B-scan ultrasound imaging are in the direction of replacing various analog gain compensating devices and display controls by an overall computerized display using digital data throughout the entire system. The present manual methods of positioning the transducer are being replaced by electronically steered and focussed transducers. Fig. 15a shows an early version of a motor-driven transducer, which could map a sector approximately 90° wide in direction. When placed at the proper positions and orientations on the chest wall, it could produce real time images of the various heart valves in motion. Fig. 15b shows a wide multielement transducer that can produce a real time image of the body section parallel to its long axis. The ultrasound beam is shifted in position from one end of the transducer to the other end to provide a linear scan over the entire width of the transducer. This is done electronically by switching the driving pulses across the transducer elements at a rate of a few hundred cycles per second.

Figs. 15c and 15d show how a multielement transducer can have its beam orientation directed and its focal length changed by the sequence of pulses delivered to the various elements. Combination of the electronically controlled deflections, as shown in Figs. 15b, c, and d, under computer control will produce in future years extremely versatile scanning machines with excellent tomographical capability.

In summary, we have reviewed in this paper advances in three clinical diagnostic imaging techniques and shown that their future development is in the direction of providing higher resolution tomography at increased speeds. The main contributor to these advances has been the availability of versatile high-speed small computers.

ACKNOWLEDGMENTS AND REFERENCES

I would like to take this opportunity thank my colleagues Drs. D. F. Boyd, R. Gould, and E. Sickles from the Radiology Department, University of California, San Francisco. The assistance of R. H. Thomas, P. Wiedenbeck, and C. Johnson-Joy of the Lawrence Berkeley Laboratory is deeply appreciated. **This work was supported by the U. S. Department of Energy under Contract W-7405-ENG-48.**

The figures listed below are reprinted with permission of Radiological Sciences, Inc: Figs. 1b and 2a.

The figures listed below are reprinted with permission of Lea and Febiger, Inc. from "Introduction to the Physics of Diagnostic Radiology" (2nd ed.) by Christensen, Curry and Nunally, copyright 1978, Lea and Febiger, Inc: Figs. 4a, 4b and 4c.

Figs. 5a, 5b, 6b and 6c were reprinted with permission of D. F. Boyd and IEEE Trans. Nuc. Sci. from the following two articles: D. F. Boyd, Status of diagnostic computer tomography, IEEE Trans. Nuc. Sci. NS-26:2836 (1979) and D. F. Boyd et al., Proposed dynamic cardiac 3-D densitometer for early detection of heart disease, IEEE Trans. Nuc. Sci. NS-26:2724 (1979).

Fig. 6a is reproduced from J. Haimson, X-ray source without moving parts for ultra-high speed tomography, IEEE Trans. Nuc. Sci. NS-26:2857 (1979).

Fig. 9 is reproduced courtesy of D. Kirsch and R. Vogel, Veterans Hospital, Denver, Colorado.

Figs. 10a and 10b are reproduced courtesy of S. Derenzo and T. F. Budinger, Donner Laboratory, Berkeley, CA.

The figures listed below are reprinted with permission of John Wiley & Sons, Inc. from "Advances in Abdominal Gray Scale Ultrasonography," B. B. Goldberg (Editor), Ch. 2 by E. N. Carlsen and G. S. Perlmutter, copyright 1977, Wiley Medical Press: Figs. 15a, 15b, 15c and 15d.

This work was supported by the Physics Research Division of the United States Department of Energy under contract no. W-7405-ENG-48.

[1] Tubes of this type manufactured by Radiological Sciences, Inc., Santa Clara, California.

[2] Private communication and picture courtesy of E. Sickles, University of California, San Francisco.

[3] D. F. Boyd, Status of diagnostic computer tomography, IEEE Trans. Nuc. Sci. NS-26:2836 (1979).

[4] R. A. Robb et al., The DSR: A high speed 3-D x-ray computer tomography system for dynamic reconstruction, IEEE Trans. Nuc. Sci. NS-26:2713 (1979).

[5] J. Haimson, X-ray source without moving parts for ultra-high speed tomography, IEEE Trans. Nuc. Sci. NS-26:2857 (1979).

[6] D. F. Boyd et al, Proposed dynamic cardiac 3-D densitometer for early detection of heart disease, IEEE Trans. Nuc. Sci. NS-26:2724 (1979).

[7] R. N. Bracewell, Strip integration in radioastronomy, Aust. J. Phys. 9:198 (1956).
[8] K. C. Tam, V. Perez-Mendez, and B. Macdonald, Reconstruction in emission and transmission tomography with limited angular input, IEEE Trans. Nuc. Sci. NS-26:2797 (1979). Also, Lawrence Berkeley Laboratory report LBL8539 (Dec. 1978).
[9] T. F. Budinger et al., Isotope distribution reconstruction from multiple gamma camera views, J. Nuc. Med. 15:480 (1974).
[10] R. A. Vogel, D. L. Kirsch, M. T. Lefree et al., Thallium-201 myocardial perfusion scintigraphy: Results of standard and multi-pinhole tomography techniques, Am. J. of Cardiology 43: 787 (1979).
[11] S. E. Derenzo, T. F. Budinger et al., The Donner 280 crystal high resolution positron tomograph, IEEE Trans. Nuc. Sci. NS-26: 2790 (1979).
[12] M. TerPogossian, M. Phelps, and E. J. Hoffman, Radiology 114: 89 (1975).
[13] Z. H. Cho, J. K. Chan, and L. Eriksson, Circular ring transverse axial positron camera for 3-D reconstruction, IEEE Trans. Nuc. Sci. NS-23:613 (1976).
[14] C. J. Thompson, E. Meyer, and Y. L. Yamamoto, "Positome II: A high efficiency P.E.T. device for dynamic studies," Proc. First Intl. Symp. on Positron Emission Tomography (Montreal, June 1978).
[15] G. Muehllehner et al., Performance parameters of a positron imaging camera, IEEE Trans. Nuc. Sci. NS-23:528 (1976).
[16] C. A. Burnham and G. L. Brownell, A multicrystal positron camera, IEEE Trans. Nuc. Sci. NS-19:201 (1972).
[17] V. Perez-Mendez, C. B. Lim et al., Characteristics of a MWPC camera for positron imaging, IEEE Trans. Nuc. Sci. NS-21:85 (1974). Also Nuc. Inst. & Methods 156:33 (1978).
[18] A. P. Jeavons and C. Cole, The proportional chamber gamma camera, IEEE Trans. Nuc. Sci. NS-25:164 (1976).
[19] G. K. Lum, V. Perez-Mendez et al., Lead-oxide glass tubing converter for gamma detection in MWPC, Lawrence Berkeley Laboratory report LBL9966 (Oct. 1979). To be published in IEEE Trans. Nuc. Sci. NS-27 (1980).
[20] A. P. Jeavons, G. Charpak, and R. Stubbs, High density lead converters, Nuc. Inst. & Methods 124:491 (1975).
[21] P. N. T. Wells, "Biomedical Ultrasonics," Academic Press (1977).

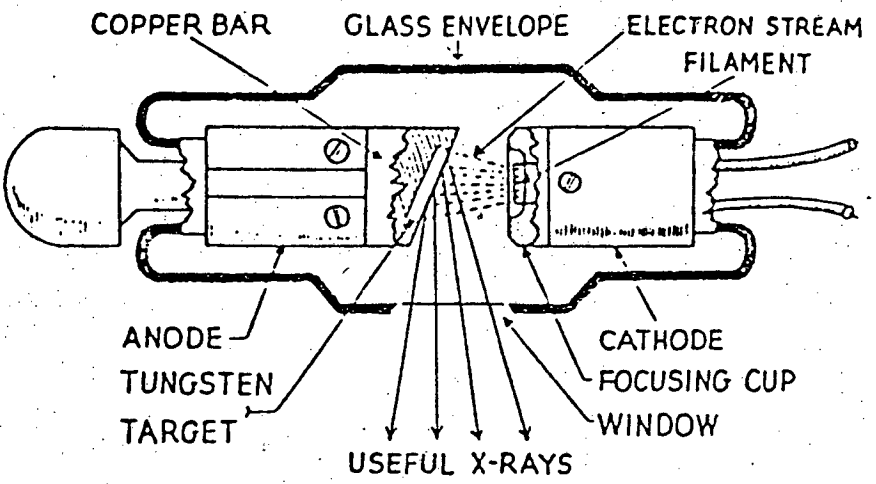

Fig. 1a. Stationary anode x-ray tube with cathode focussing cup.

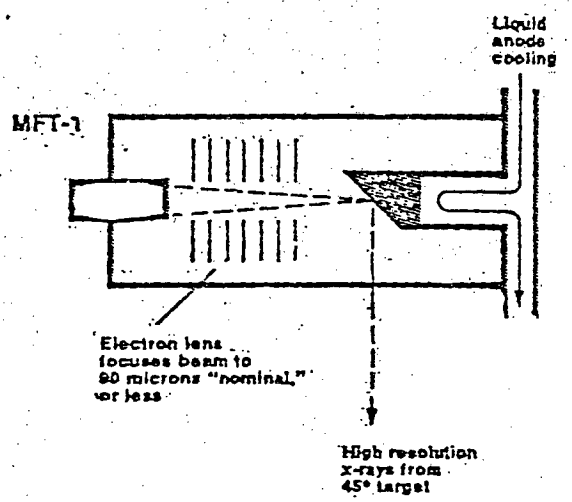

Fig. 1b. Fine focus tube with electron lens focussing.

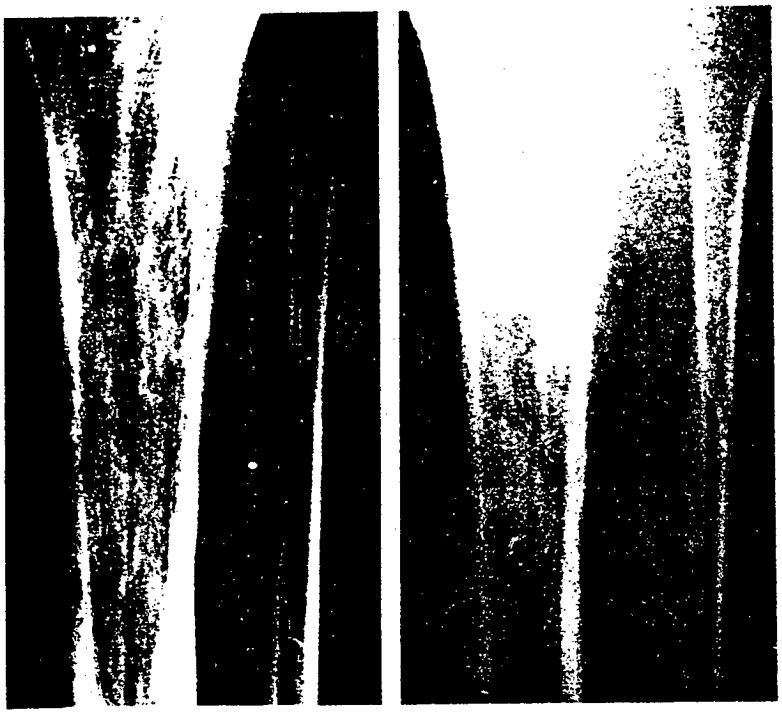

Fig. 2a. Comparison bone structure: conventional and fine focus tube.

Fig. 2b. Radiogram for breast cancer calcifications: fine focus tube.

XBB 792-2230A

Transmission: X-Ray

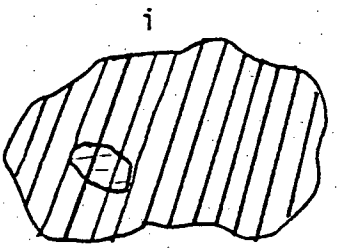

$$\rho(x,y,z) = \sum_i \rho_i(x,y)$$

Anatomy

Density altered by tumors, cysts.

Emission: Gamma Rays

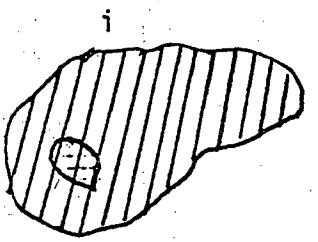

$$C(x,y,z) = \sum_i C_i(x,y)$$

Physiology

Concentration of radioisotope altered by t mors, cysts.

Ultrasound: B-Scan

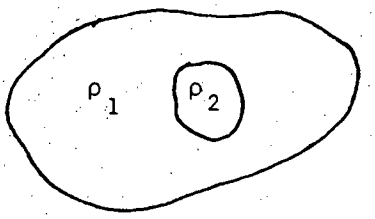

Anatomy and Tissue Characteristics

Cyst or tumor produces density boundary.

Fig. 3. Comparison of various tomographic imaging modalities.

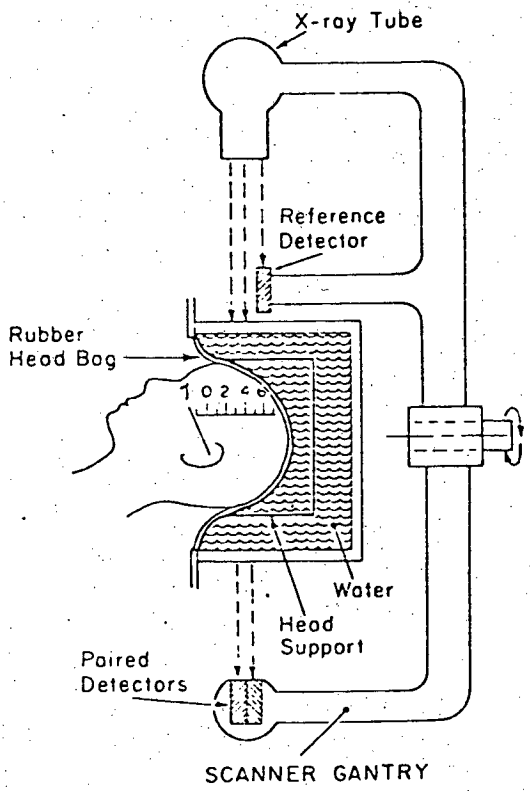

Fig. 4a. Early version of E.M.I. head scanner.

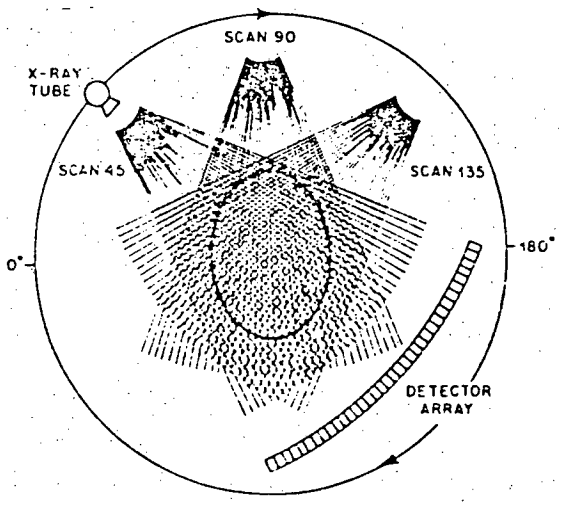

Fig. 4b. Third generation scanner: rotating x-ray tube coupled to rotating detector array.

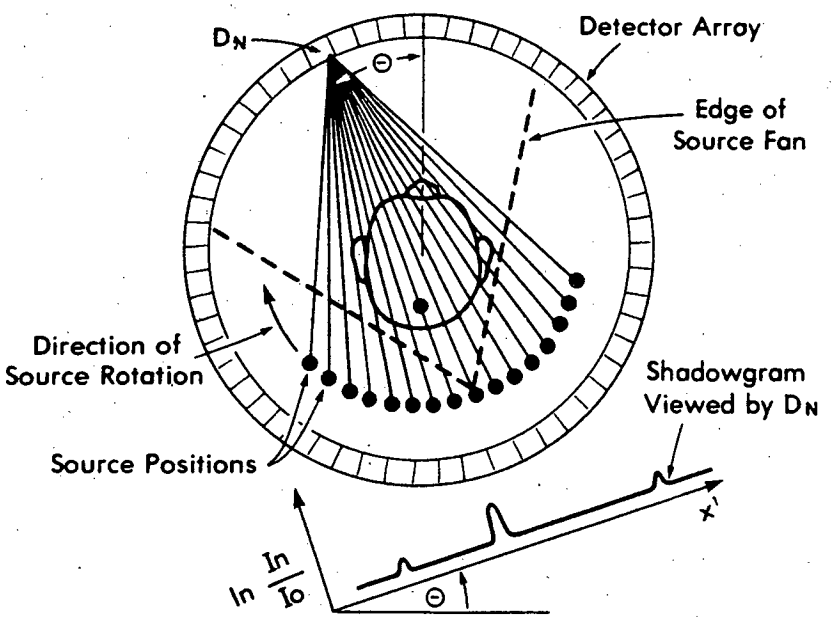

Fig. 4c. Fourth generation scanner: rotating x-ray tube: fixed detectors.

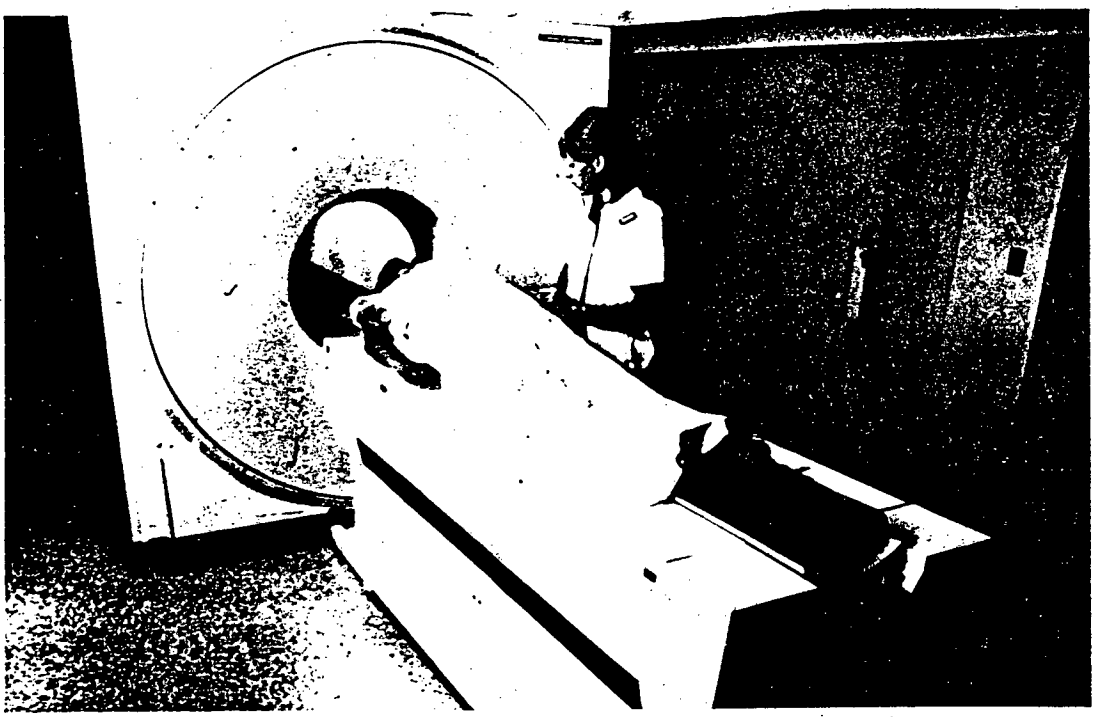

Fig. 5a. General Electric scanner. X-ray tube and detectors in circular gantry.

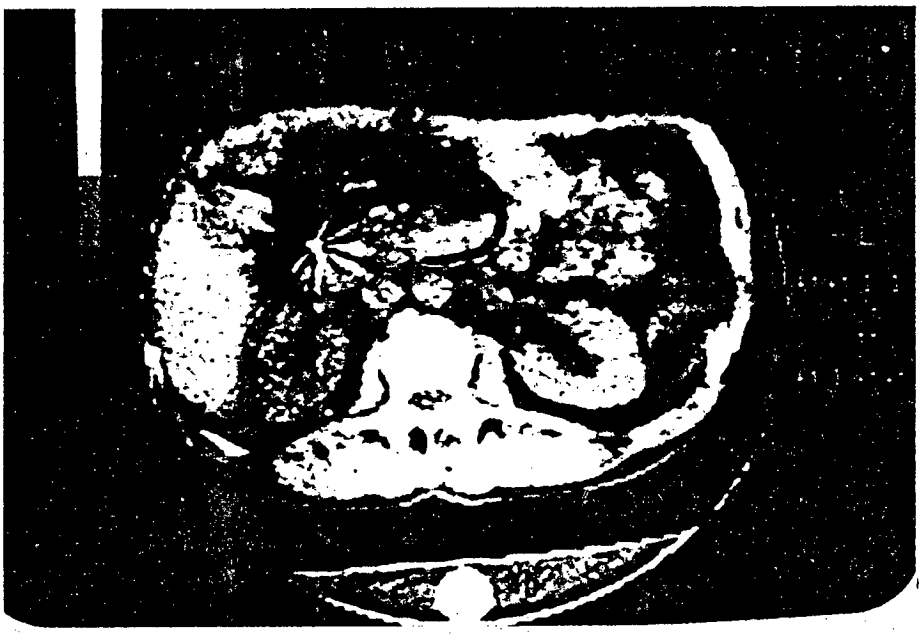

Fig. 5b. Representative tomographic scan showing artifacts produced by metal clip in patient's body.

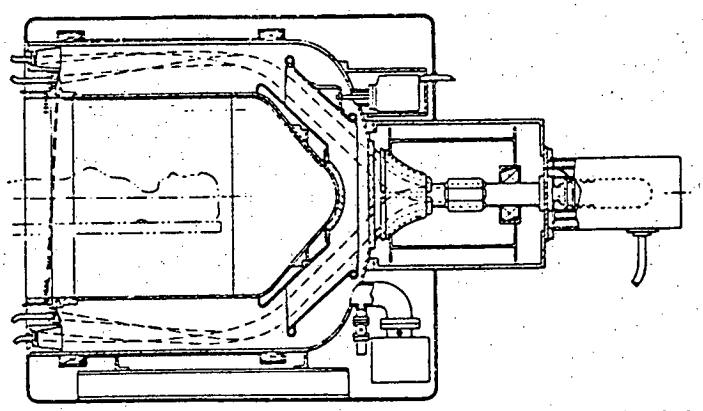

Scanner Showing Beam Transfer from Shielded Annular Standby Collector to Target.

Fig. 6a. Rotating electron beam scanner. 2π rotation.

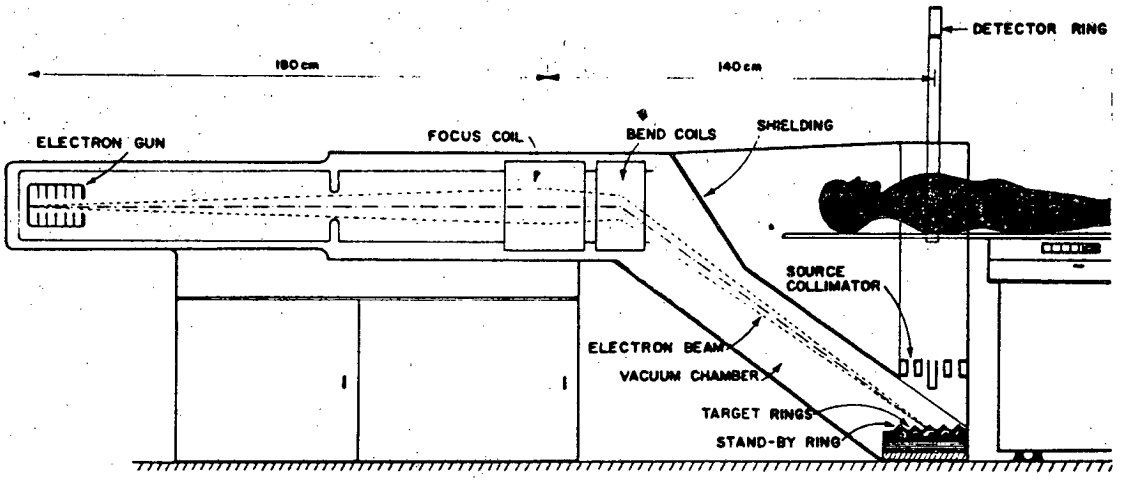

Fig. 6b. Rotating electron beam scanner. π rotation only.

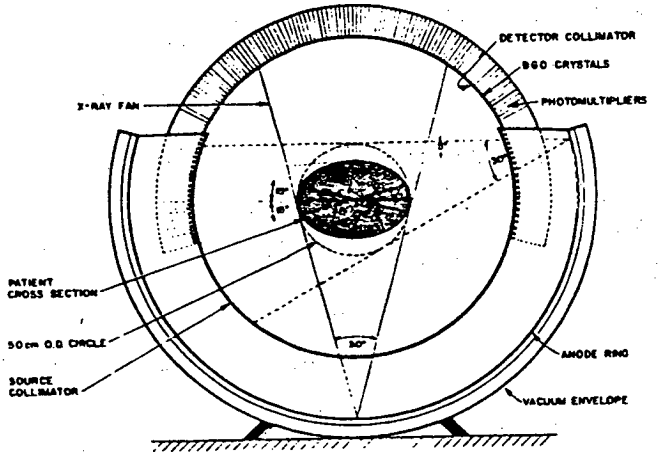

Fig. 6c. End view of π rotation scanner showing overlapping anode detector ring and scanning x-ray beam fan geometry.

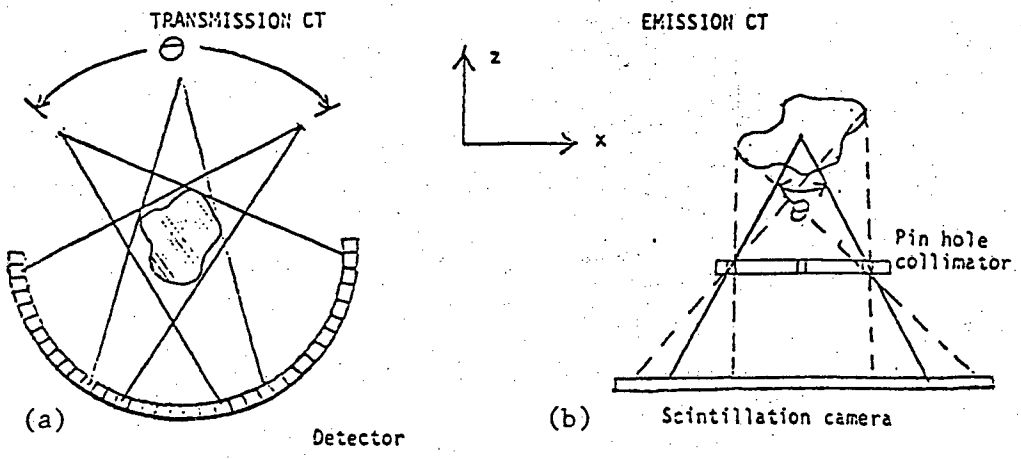

Fig. 7a. Limited-angle transmission C.T. showing fan beam and sector of fixed detectors.

Fig. 7b. Limited-angle emission tomography, using discrete pinhole collimator.

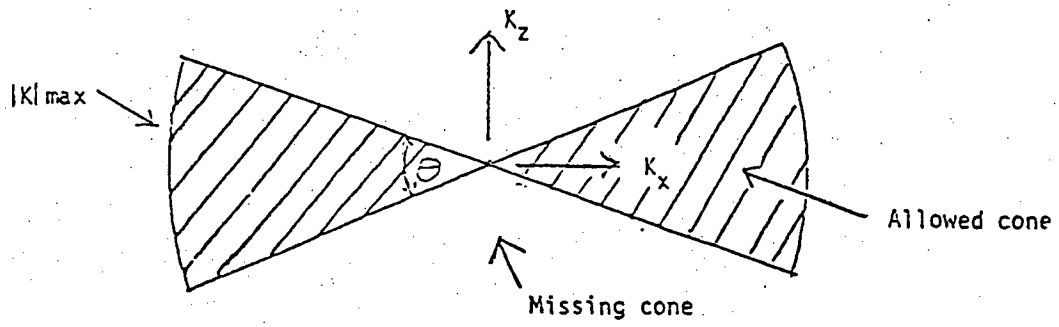

Fig. 7c. Fourier space representation showing components in "allowed cone" corresponding to the limited-angle imaging in geometry in Figs. 7a and b.

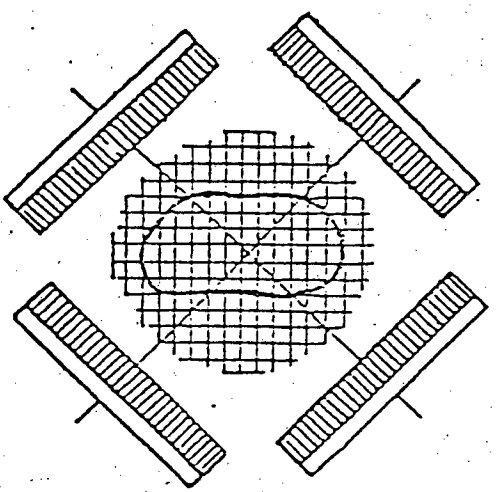

Fig. 8a. Schematic of 2π emission tomography using rotating scintillation camera with parallel-hole collimator.

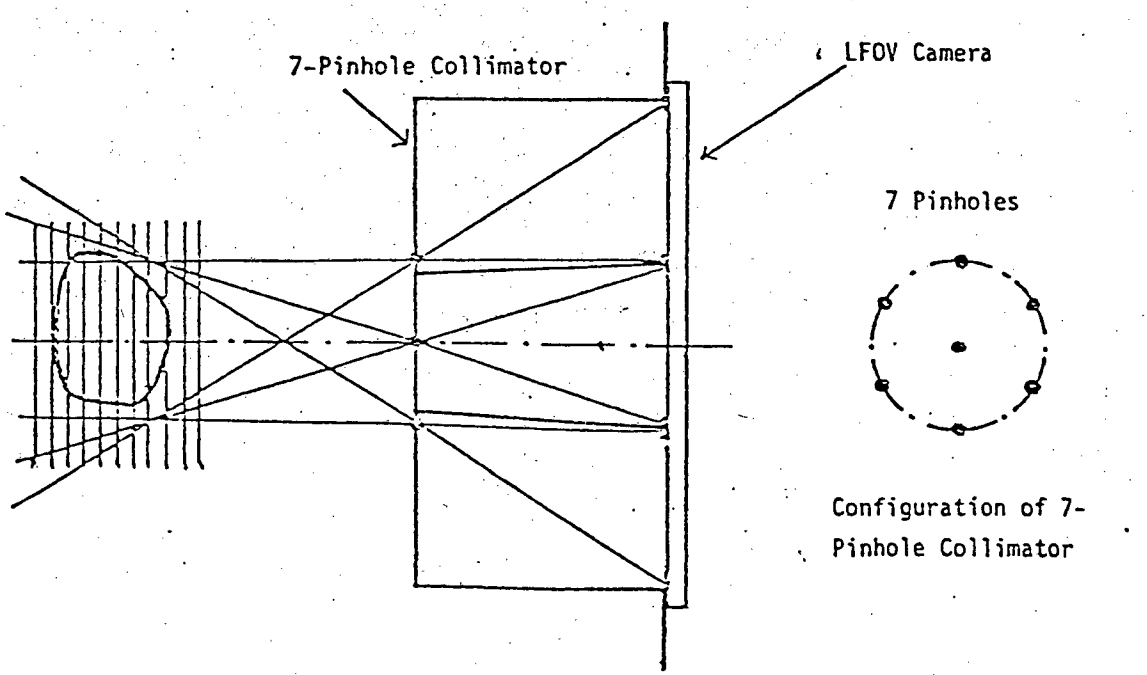

Fig. 8b. Schematic of limited-angle emission tomography using large stationary scintillation camera and 7-pinhole collimator.

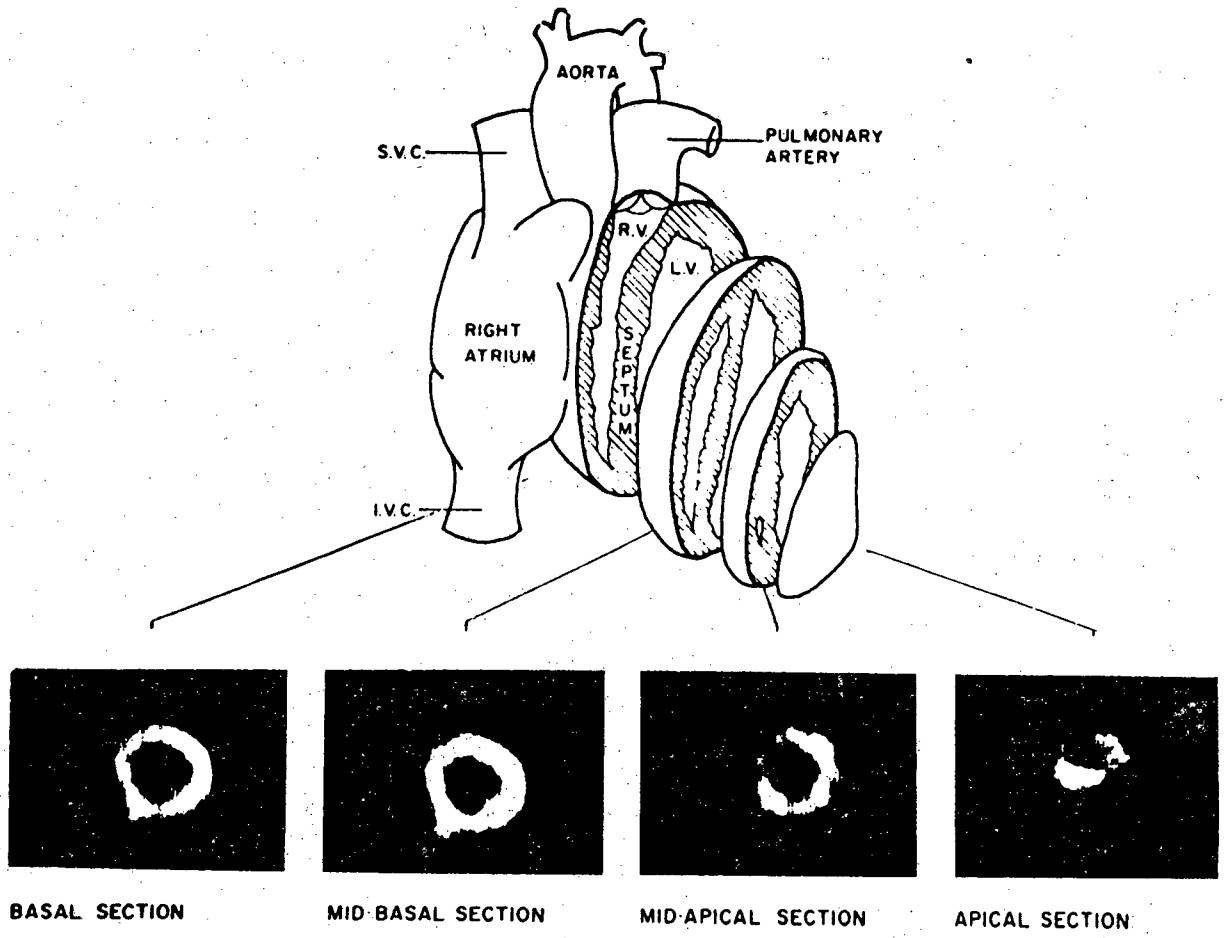

Fig. 9. Emission tomography using 7-pinhole collimator. Heart imaging with ^{201}Tl. Heart anatomy and four corresponding tomograms are shown. Picture taken by Denver Veterans Administration Hospital Nuclear Medicine group.

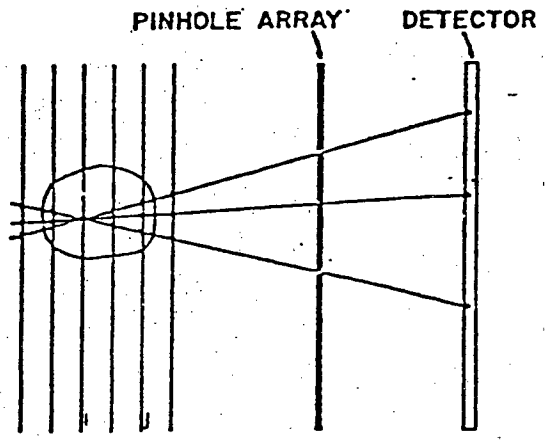

Fig. 10a. Single-photon imaging collimator.

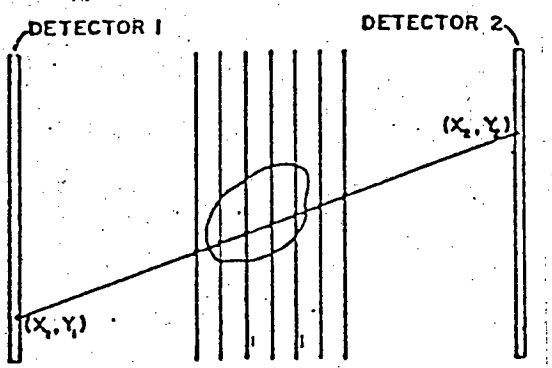

Fig. 10b. Positron imaging. Area detectors. No collimator.

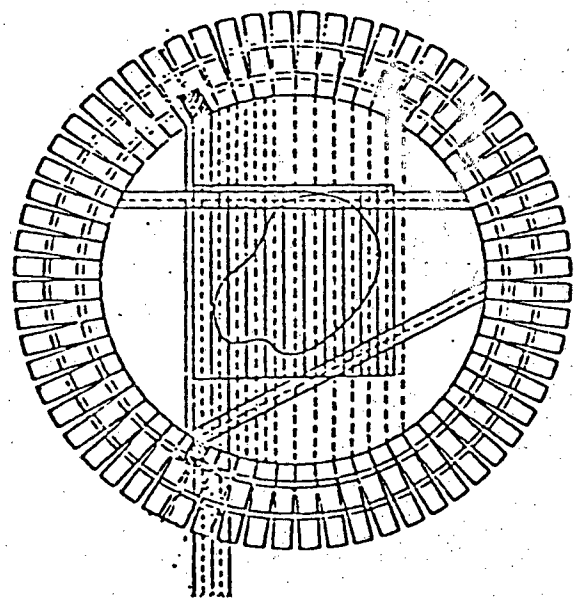

Fig. 10c. Positron imaging. Single slice. NaI ring detector.

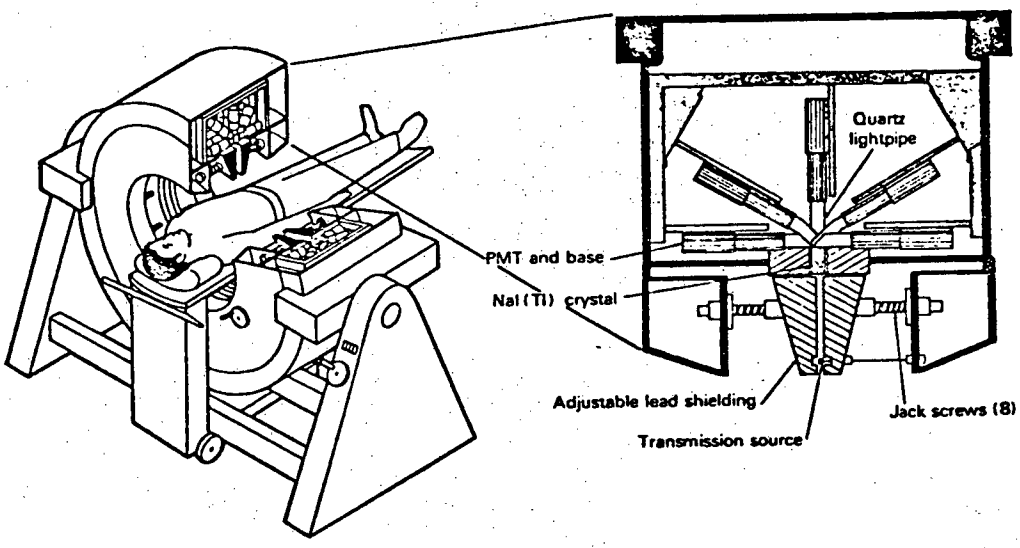

Fig. 11a. Schematic of Donner Laboratory 280 crystal positron camera showing NaI crystal mounts, light pipes and P.M. tubes.

Fig. 11b. Transmission (left) and emission pictures of heart, taken with Donner camera. Images taken with ^{82}Rb for a total of 1.5 x 10^6 true counts.

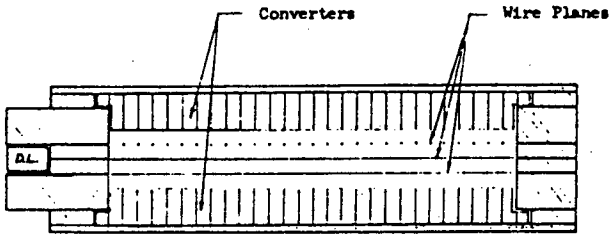

Fig. 12a. Cross section of MWPC gamma detector showing lead converters and wire planes.

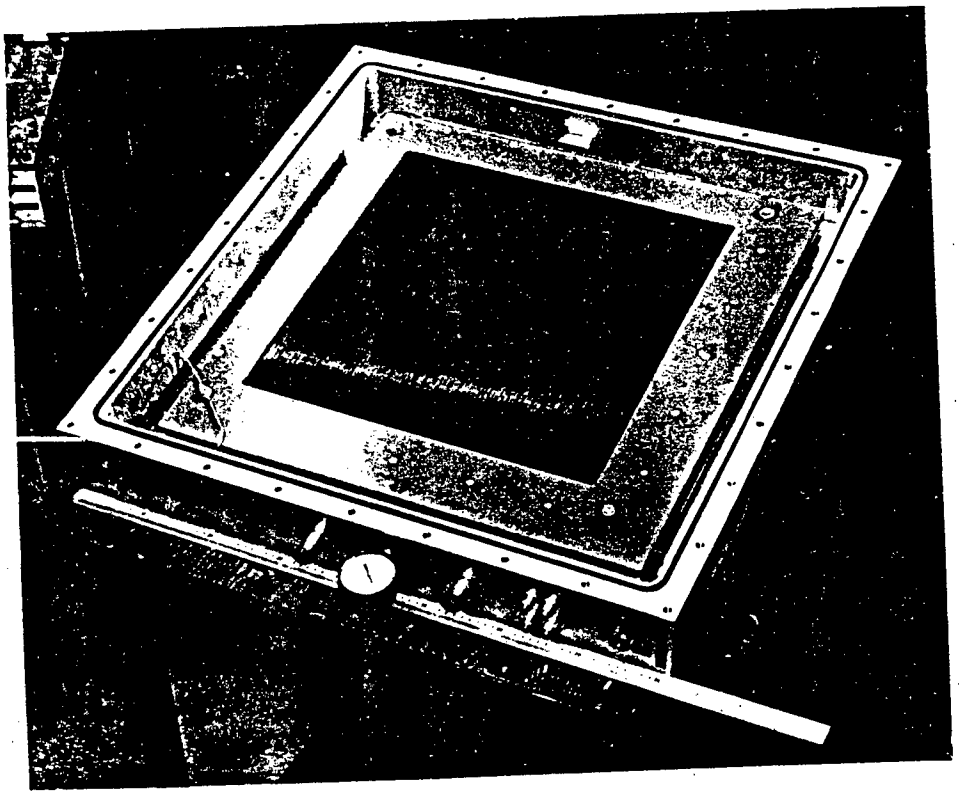

Fig. 12b. Photograph of MWPC chamber showing wire planes and lead converter below.

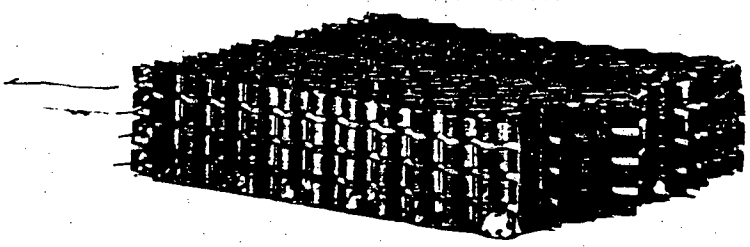

Fig. 12c. Photograph of honeycomb lead converter showing plated lead bands on plastic support structure.

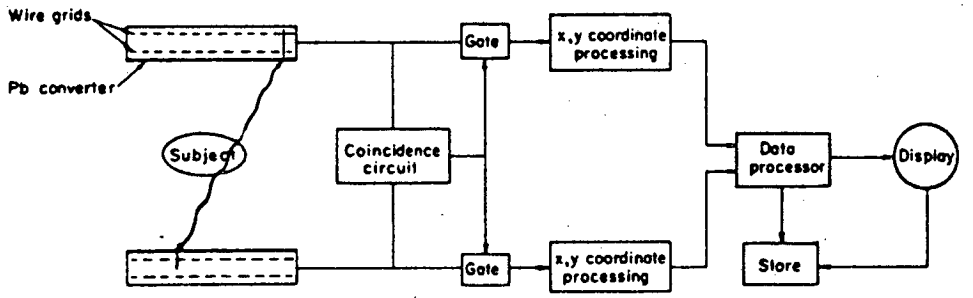

Fig. 13a. Schematic of two area detectors MWPC positron camera showing electronic logic.

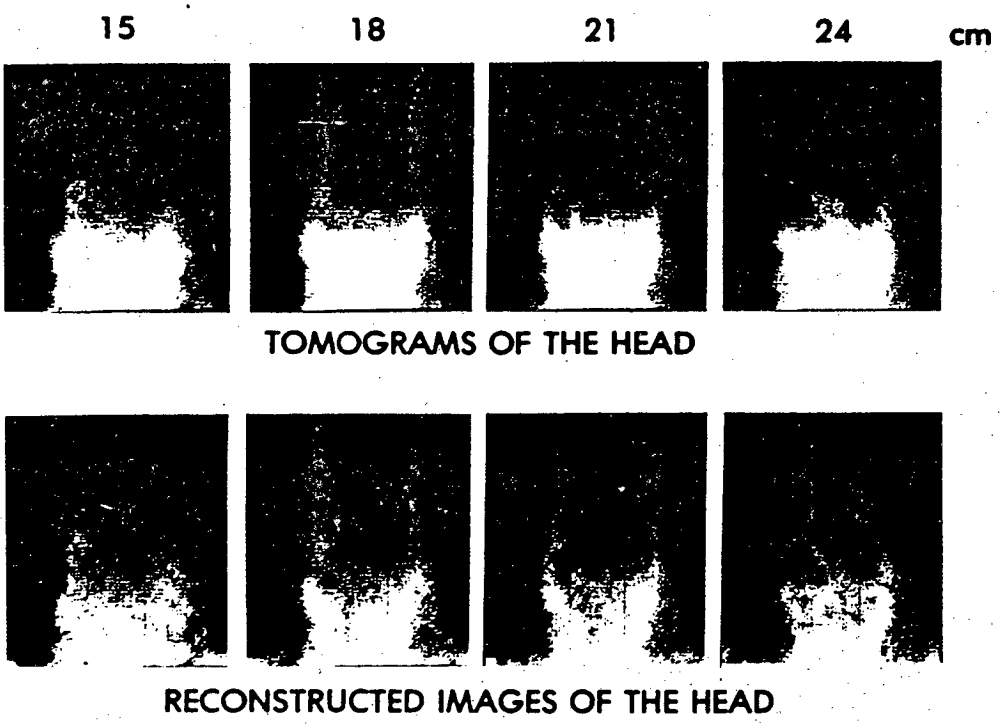

Fig. 13b. Representative tomograms of head showing tumor on left side taken with MWPC camera. Images are displayed by two different reconstruction algorithms.

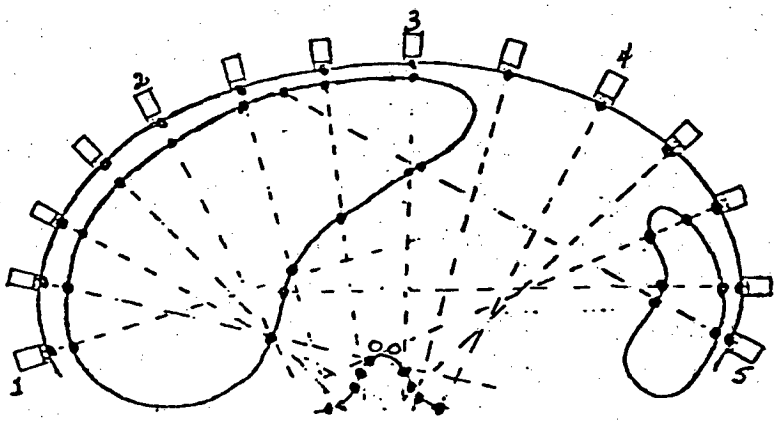

Fig. 14a. Successive positions of ultrasound transducer during transverse B-scan of abdomen.

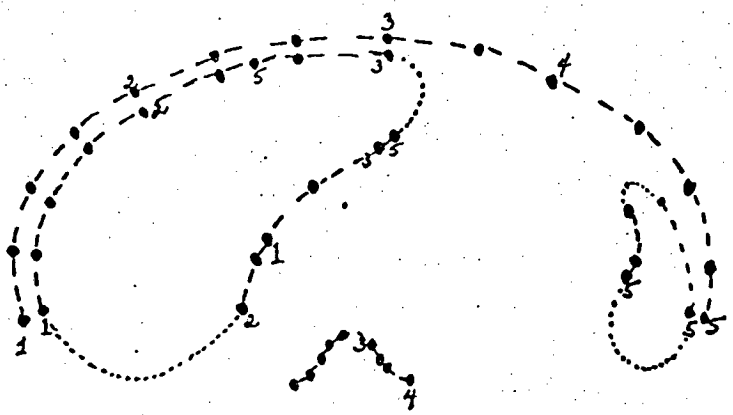

Fig. 14b. Summation of multiple light spots in transverse B-scan showing how image is formed.

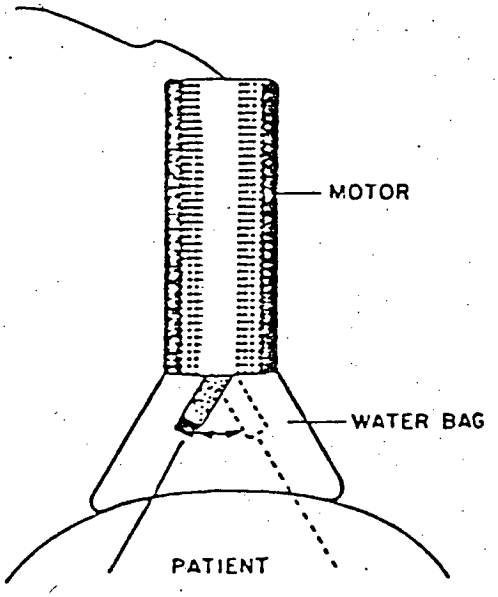

Fig. 15a. Oscillating sector scanner for real-time viewing of heart valve motion.

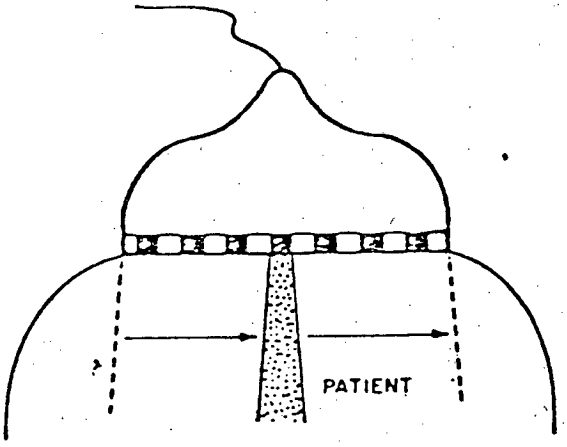

Fig. 15b. Electronically switched linear array. Transducer beam is programmed to scan entire area without mechanical motion.

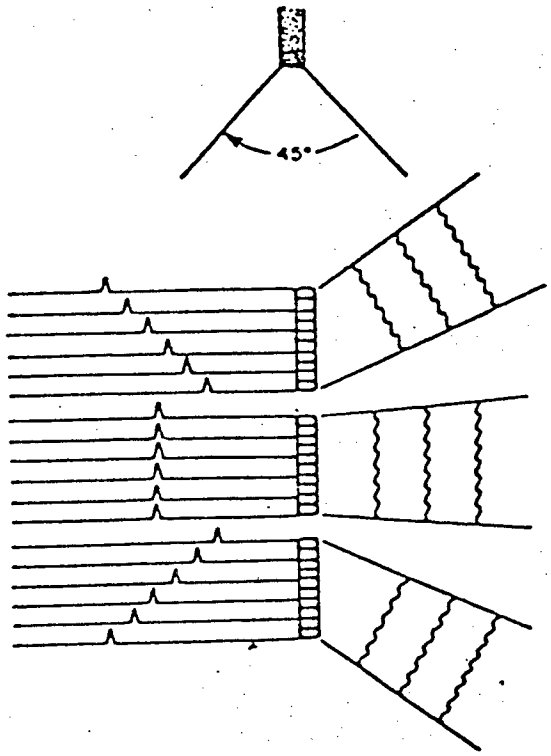

Fig. 15c. Electronically switched linear array to provide different scan directions by phase changes in triggering sequence.

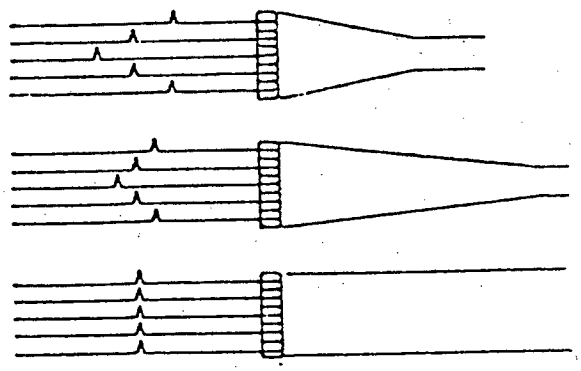

Fig. 15d. Dynamic focussing produced by programmed phasing of triggering sequence.

This report was done with support from the Department of Energy. Any conclusions or opinions expressed in this report represent solely those of the author(s) and not necessarily those of The Regents of the University of California, the Lawrence Berkeley Laboratory or the Department of Energy.

Reference to a company or product name does not imply approval or recommendation of the product by the University of California or the U.S. Department of Energy to the exclusion of others that may be suitable.

TECHNICAL INFORMATION DEPARTMENT
LAWRENCE BERKELEY LABORATORY
UNIVERSITY OF CALIFORNIA
BERKELEY, CALIFORNIA 94720